HIGH LATITUDE IONOSPHERIC IRREGULARITY DETECTION USING COSMIC RADIO OCCULTATION OBSERVATIONS

6.7

M. Feng and S. Skone
Department of Geomatics Engineering, Schulich School of Engineering University of Calgary, Canada

BIOGRAPHY

Man Feng is an MSc Student in the Department of Geomatics Engineering at the University of Calgary. She received her first Masters degree (2007) in Space Physics at the Peking University, China. She received her B.S. (2004) in Computer Science and Technology at the Tianjin University, China.

Susan Skone, Ph.D., is an Associate Professor in the Department of Geomatics Engineering, Schulich School of Engineering, at the University of Calgary. She has a background in space physics and conducts research in ionospheric and tropospheric effects on GNSS. She has developed software for mitigation of atmospheric effects and is currently chair of the Canadian Navigation Society.

ABSTRACT

High latitude ionospheric scintillations are a concern for satellite-based navigation systems. This paper analyzes electron density distributions in the high latitude disturbed ionosphere using COSMIC radio occultation (RO) observations. Analyses are based on the COSMIC level 2 product: retrieved ionospheric electron density profiles. A polynomial approximation is used to filter the vertical electron density profiles and identify small-scale ionospheric disturbances. Electron density profiles provide valuable information about the spatial variations and altitude distributions of structures in the ionosphere.

Average electron density values for high latitudes are also generated as a function of altitude and latitude for nighttime sectors. Geomagnetically disturbed days and quiet days are picked for comparison. Typical auroral radio occultation (RO) events are selected for validation. Selected electron density profiles have enhancements at approximately 110 km altitude due to auroral E-ionization (AEI.) Results of the filtering provide the altitude distribution and power density information for ionospheric structures and associated instabilities.

Power spectral analysis is also applied to electron density profiles to infer vertical scale sizes of ionospheric structures. The spatial distribution of E-region electron density structures is studied for disturbed periods and correlation with auroral region boundaries is demonstrated.

Overall it is determined that the presence of auroral ionospheric irregularities can be detected using COSMIC RO observations. Such irregularities can be associated with significant scintillation effects for Global Navigation Satellite Systems (GNSS). COSMIC is a powerful tool for practical applications in GNSS space weather monitoring.

Man Feng, University of Calgary, Dept. of Geomatics Engineering, Calgary, Alberta, T2N1N4, e-mail: m.feng@ucalgary.ca

INTRODUCTION

Ionospheric electron density irregularities can cause short-term fading and rapid phase changes of GPS L1 and L2 signals [Mitchell et al. 2005]. The formation of irregularities is usually associated with some specific ionospheric activity dependent on location and local time. During strong “storm” periods the mid-latitude region can experience storm enhanced densities and subauroral ionospheric drifts [Ledvina et al. 2004]. At high latitudes, such as Canada, usually the auroral oval and polar cap regions are affected by the related magnetospheric processes [Basu et al., 2002]. Recently GPS radio occultation techniques (GPS/MET, CHAMP, COSMIC, GRACE missions etc.) - which provide observations of the ionosphere from geospace - are deemed to be useful tools for monitoring the ionospheric structures at different layers [Tsybulya, 2005; Wu 2006].

The COSMIC (Constellation Observing System for Meteorology Ionosphere and Climate) is a six identical FORMOSAT-3 satellite mission [Schreiner et al. 2007; Anthes et al., 2008]. COSMIC commenced its operations from 15 April 2006. Around 2500 globally distributed occultation events are provided each day which offer much better spatial coverage than the former RO missions. COSMIC satellites’ altitude is also higher than CHAMP, which results in possible observations at higher F2 layer altitudes. A comparison of COSMIC and CHAMP for one day of observations is shown in Figure 1. In this study the database of RO is obtained from COSMIC post processed data at http://cosmic-io.cosmic.ucar.edu/cdaac.

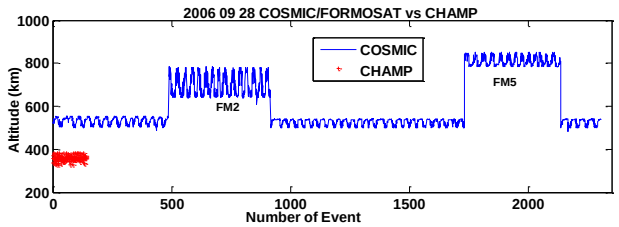

Figure 1 Top altitude for 1Hz level 2 products for COSMIC and CHAMP on 28 September 2006

In this work the COSMIC level 2 “ionPrf” product is used. It is obtained from a single patch antenna at 1 Hz sample

frequency with data recorded at altitudes below 600 km to 800 km. The retrieved parameter is the calibrated TEC. The inversion algorithm to obtain electron density profiles is described by Schreiner et al. [1999]. Refraction of the radio wave between a GPS satellite and the LEO causes excess phase delay which is then used to calculate the calibrated TEC. Retrieved electron density profile plus tangent points' altitude, longitude, and latitude are recorded in "ionPrf". Days of interest are selected with sufficient observations available in the Canadian longitude sector near local midnight. The objective of this paper is to study RO events for disturbed auroral nighttime periods and establish spatial characteristics of ionospheric electron density structures. Statistical maps of ionospheric structures are created by averaging electron density measurements from observations for several auroral nighttime locations.

AURORAL PHENOMENA

The auroral oval is a region of closed magnetic field lines, which is characterized by high conductivity, auroral electroject currents and precipitating electrons. Under active conditions, energy from solar wind is released into the auroral ionosphere and the precipitating electrons collide with neutral atmospheric constituents at around 110 km altitude, resulting in visible aurora and variable total electron content (TEC). The magnetosphere shields the Earth's magnetic field from the solar wind and the energetic particles do not enter the ionosphere directly. The particles will precipitate into the auroral oval along the magnetic field lines. The electrons are transported through the field-aligned currents (Figure 2) and into the electroject region which is colocated with the auroral oval. Formation of the substorm current wedge is a characteristic of the auroral substorm phenomenon. The localized closure current can be observed by ground-based magnetometers in perturbations of the H (north-south) component.

The enhancement of electron density at altitudes near 110 km and in the range 65-75 deg N geomagnetic latitude after local midnight (e.g. Figure 6) is associated with auroral substorm activity. Auroral precipitation creates irregularities in the E region - often called Auroral E-ionization (AEI) [Skone, 1998]. Small-scale variations corresponding to the localized current structures in the auroral ionosphere result in localized enhancement of auroral total electron content (TEC) [Hunsucker et al.1995]. Ionospheric electron density structures and irregularities exist with horizontal scale sizes in the range 20 to 400 km [Baron, 1974]. Decorrelation of TEC and GPS ionospheric range delays can occur over short distances (tens of kilometers). AEI can have magnitudes comparable to the F region maximum with electron densities in the range 2 – 20 $\times 10^{11}$el/m^3 [Baron, 1974].

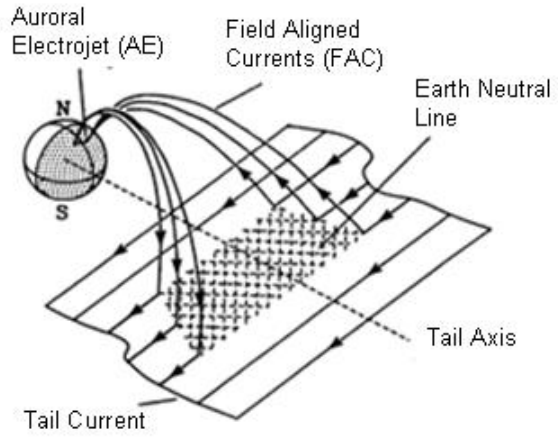

Figure 2 Auroral substorm current wedge; the current closes westward through the ionosphere at approximately 110 km altitude

DATA SETS

In this paper magnetic activity is inferred from local magnetometer observations and K indices in addition to the global Kp index. Magnetic K indices are available from NOAA [NOAA, 2009]. There are three databases for magnetometer network observations. One is available from GSC (Geological Survey of Canada) at http://geomag.nrcan.gc.ca and another is available from CSSDP (Canadian Space Science Data Portal) at http://portal.cssdp.ca. Site locations of GSC and CSSDP magnetometers are shown in Figures 3 and 4 respectively. Figure 4 shows CARISMA (Canadian Array for Realtime Investigations of Magnetic Activity) from CSSDP. Another magnetometer array located in Alaska is called GIMA (Geophysical Institute Magnetometer Array); this will also be used to identify disturbed ionospheric conditions.

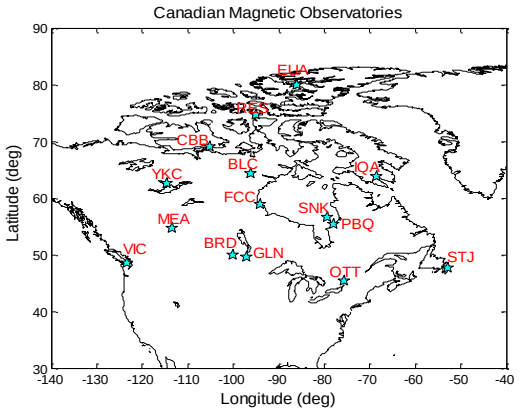

Figure 3 Geographic locations of GSC magnetometers.

Since 2003 the University of Calgary has operated several GPS scintillation receivers in Canada. Scintillation indices and raw GPS data are continuously recorded at three GPS receivers in the CANGIM (CANadian GPS Network for Ionosphere Monitoring). These receivers are NovAtel Euro4 and capable of deriving phase and amplitude

scintillation information. Figure 5 shows their locations. Three stations are aligned approximately along the same meridian at latitudes spanning the sub-auroral, auroral and polar cap regions depending on ionospheric activity level. Yellowknife is a high latitude site where aurora is commonly to be observed while Calgary and Athabasca are primarily within the subauroral region. Nightside auroral scintillation effects will be defined from the extensive CANGIM GPS data set.

In this work both the magnetometer networks and CANGIM ground-based scintillation observations are used to infer the level of geomagnetic activity and associated irregularities in the ionosphere.

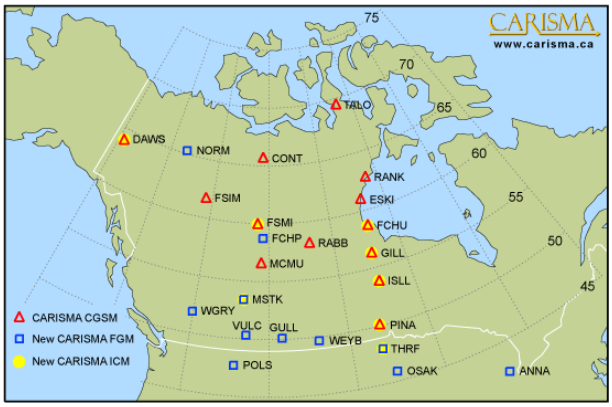

Figure 4 Geographic locations of CARISMA magnetometers [CARISMA, 2009]

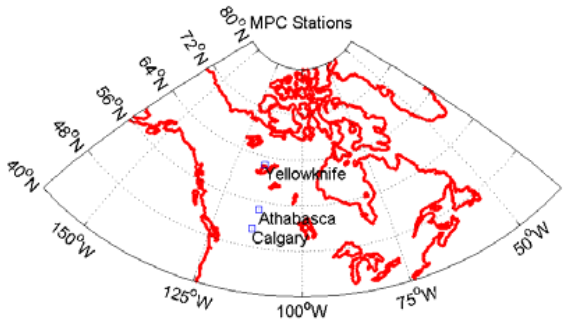

Figure 5 Geographic locations of three GPS scintillation receivers: Calgary, Athabasca, Yellowknife [Skone et al., 2008]

Figure 6 shows the electron density profiles derived from COSMIC observations on 2 September 2007 as a function of geomagnetic latitude and altitude. This was a magnetically disturbed day with K index values (Alaska) greater than five for the periods studied [NOAA, 2009]. The dataset was selected by choosing RO events with tangent points located in the longitude sector from 60 deg W to 160 deg W and nightside local times. The longitude sector is chosen based on magnetometer observations from GIMA, CARISMA, and GSC; magnetic time series at Alaska and the other two networks showed significant magnetic field fluctuations in the local time range 0000 LT to 0400 LT on this day [GIMA, 2009; GSC, 2009; CARISMA, 2009].

Available data within grid sectors of the same latitude and altitude range are combined and averaged to derive the electron density values. The vacant sectors in the figures are due to lack of RO observations. An enhancement of electron density is observed at auroral oval latitudes in the E region.

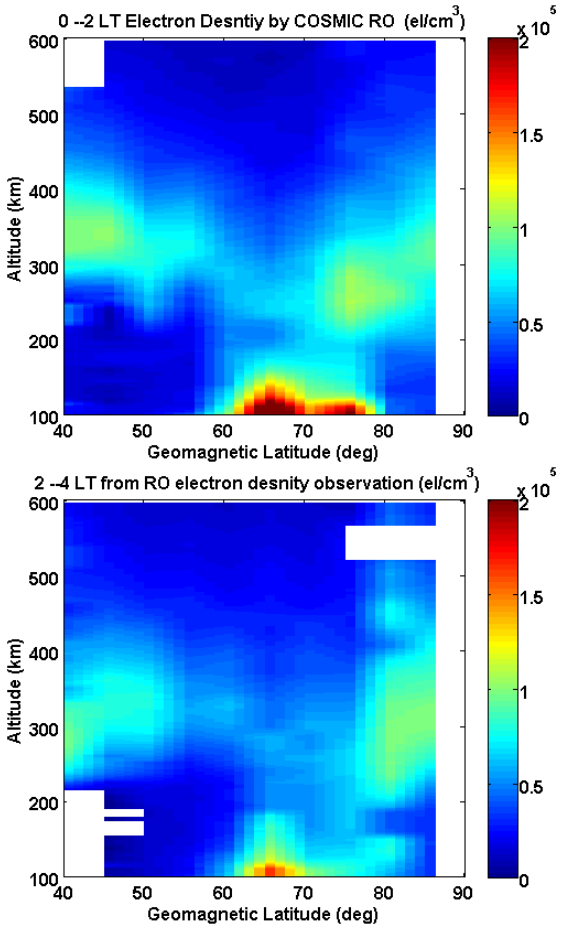

Figure 6 Average electron density values 0000-0200 LT (top) and 0200-0400 LT (bottom) 2 September 2007

Plots in Figure 6 show strong electron density enhancements in the range 60-80 deg N geomagnetic latitude near 110 km altitude with largest values in the sector 0000-0200 LT . The density enhancement reaches values greater than 2×10^5 el/cm^3. Similar plots are generated for a quiet day (8 December 2007) in Figure 7 for comparison purposes. The planetary Kp index was zero for the whole quiet day [NOAA, 2009]. In contrast to Figure 6, no large E-region electron density enhancement exists. Typical F-region electron density peaks are observed.

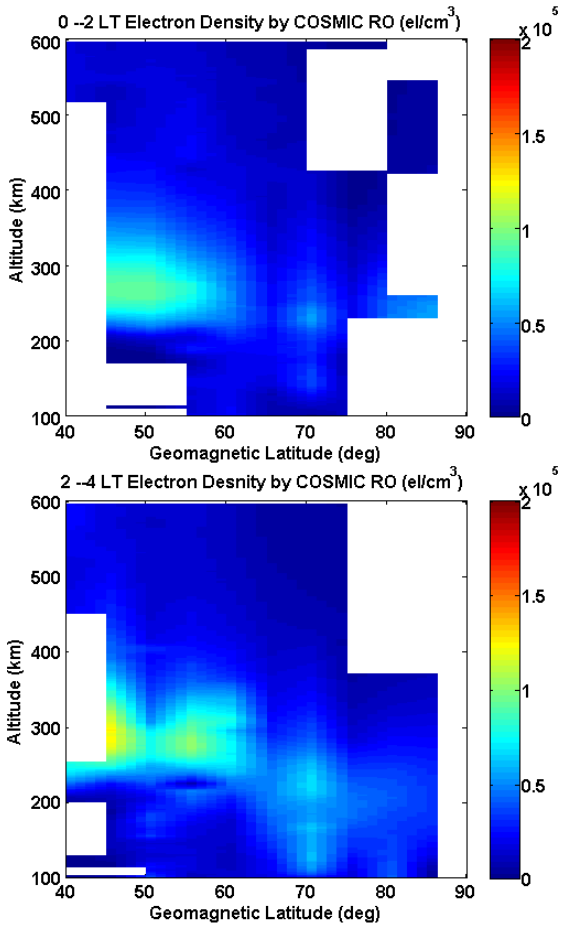

Figure 7 Electron density values 0000-0200 LT (top) and 0200-0400 LT (bottom) 8 December 2007

In the previous example (Figure 6) E-region electron density enhancements observed from COSMIC RO observations are consistent with patterns of energetic electron precipitation expected for auroral substorm phenomena. Note that the electron density plots (Figures 6 and 7) are created by averaging observations from different longitude sectors; future expanded radio occultation missions are expected to achieve instantaneous global coverage with full local time sector coverage and resolution high enough to monitor ionospheric disturbed conditions continuously.

AURORAL RADIO OCCULTATION EVENTS

Two events are selected for auroral substorm periods, as detected by magnetometer observations, in which RO observations are available at auroral oval latitudes. The tangent points of RO profiles are shown as blue lines in Figure 8.

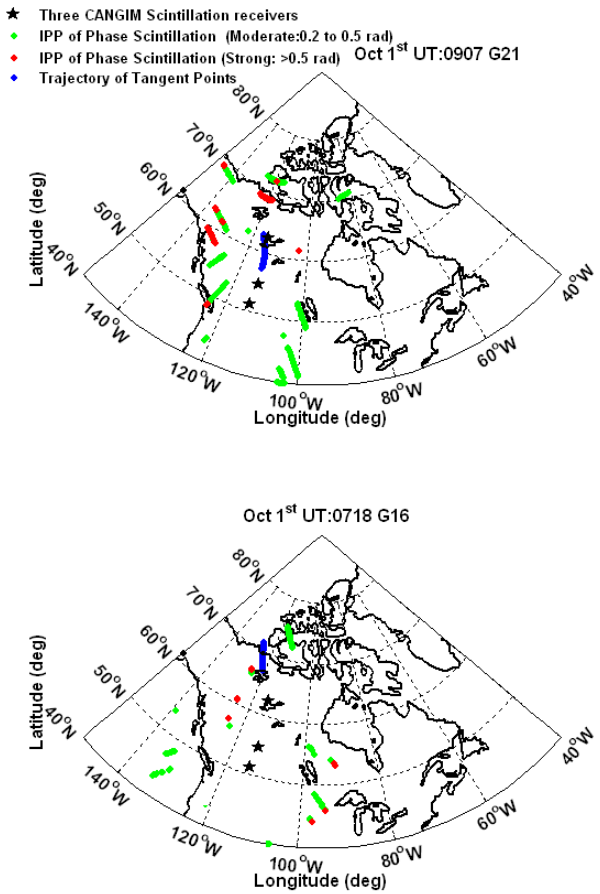

Figure 8 Two COSMIC RO auroral events during disturbed periods with tangent points (blue) and CANGIM ionospheric pierce points (IPP) with phase scintillation observations in the range 0.2 rad – 0.5 rad (green) and larger than 0.5 rad (red).

CANGIM scintillation IPP points are also shown in green (moderate phase scintillation in the range 0.2-0.5 rad) and red (strong phase scintillation larger than 0.5 rad) [Yu, 2007]. RO tangent points are within the area of observed scintillation. Figure 9 shows a time series of phase scintillation observed at Yellowknife. RO profiles are available during the two periods of strong scintillation. It is expected that ionospheric irregularities exist at these times.

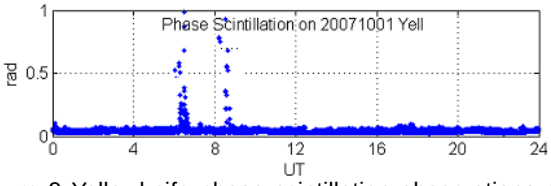

Figure 9 Yellowknife phase scintillation observations on 1 October 2007

Figure 10 shows electron density profiles for the two auroral events. An AEI feature is observed around 110 km altitude. Figure 11 is an electron density profile at local midnight during an ionospherically quiet period for comparison purposes. No AEI feature is observed in Figure

11. And the density peak for the quiet data is at altitudes above 200 km in the F region.

Figures 10 and 11 also show the filtered electron density profiles for smaller scale sizes in which ionospheric disturbances can be identified. In this analysis a nine-point cubic polynomial approximation is applied to the full COSMIC electron density profile in order to remove the large-scale structures (low frequency trend) and show detailed information about small-scale ionospheric disturbances. A similar filter is applied by Tsybulya and Jakowski [2005] for TEC measurements during a RO event. The polynomial approximation to electron density observations is conducted along with the RO TPD (tangent point displacement); the polynomial is then subtracted from the original electron density profile. The remaining high frequency components are then mapped to altitude.

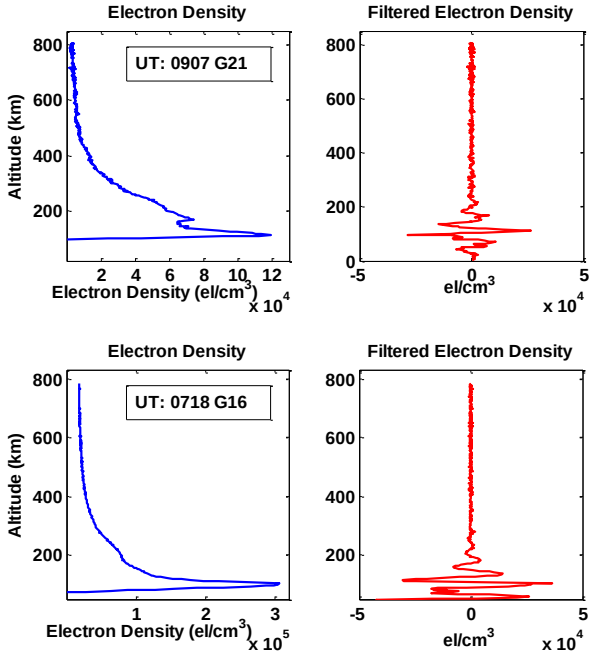

Figure 10 Electron density profiles (left) and corresponding filtered profiles (right) for the two auroral RO events on 1 October 2007.

After filtering, only structures with vertical scale sizes less than approximately 20 km remain. The filtered results for the second event (bottom plot of Figure 10) show that the electron density can have fluctuations of 3×10^4 el/cm^3 for vertical scale sizes of 10 km. For the two auroral events it can be observed that the E-region enhancements and structures developing from energetic electron precipitation are dominant while the F-region variations are only a few percent of the background values. Large phase scintillation values observed at the Yellowknife CANGIM station are consistent with E-region irregularities developing from energetic electron precipitation.

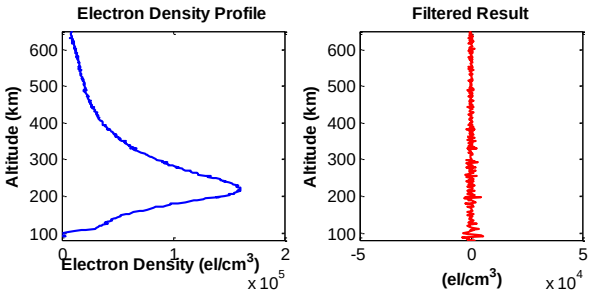

Figure 11 COSMIC electron density product for RO on 24 August 2007

Power spectral density analysis is also conducted for the electron density profiles in Figures 10 and 11. An alternative technique to the Fast Fourier Transform called the “Lomb method” is chosen to conduct the power spectral analysis. For the “Lomb method” [Lomb, 1976] the power spectral densities are derived from least squares adjustments to compute parameters for each wave number. The Lombscargle method is chosen since RO measurements have unequal spatial sample intervals in altitude.

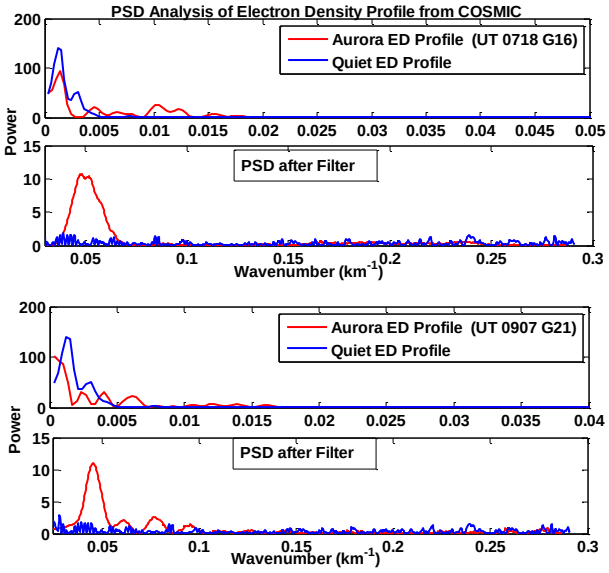

Figure 12 Power spectral densities of electron density profiles for the two selected auroral events compared with quiet period.

Figure 12 shows the power spectral density analysis. For each event the top plot shows the power spectral analysis for wave numbers smaller than 0.05 km^{-1} (wavelengths larger than 20 km). The lower plot is for higher wave numbers. The electron density profile for the quiet day is dominated by major peaks at less than 0.005 km^{-1} which corresponds to a wavelength of 200 km.

From analysis of the two auroral scintillation events it is observed that electron density structures with scale sizes in the range 50-100 km exist in the disturbed ionosphere. The lower plot for each event is the power spectral density for small wavelength ranges. A prominent feature in these

electron density profiles is a dominant peak observed around 0.05 km^{-1}; this wavenumber corresponds to wavelength of 20 km. There is no significant difference in the disturbed and quiet power spectral densities for wavelengths less than 10 km (wave numbers greater than 0.1 km^{-1}).

Note that the power spectral density analysis of ionospheric structures is limited by the vertical resolution of the RO measurements. COSMIC RO observations are available with spatial sample intervals from 1 km to 3 km. Additionally the true size of ionospheric electron density structures differs from the size inferred from tangent point locations. However, since the major fluctuations for these two auroral events arise from the energetic electron precipitation in the E layer the dominant peak around 20 km wavelength probably arises from AEI at 110 km with a vertical scale size of 10-20 km (Figure 10).

ANALYSIS OF 4-7 DECEMBER 2008 IONOSPHERIC DISTURBANCES

In Figure 13 magnetometer observations between 1000 and 1200 UT in Alaska show decreases in the H component consistent with the presence of an enhanced westward electrojet – and auroral substorm events. Based on GIMA observations in Figure 13 it can be determined that the ionosphere is disturbed 1000-1200 UT; this corresponds to 0000-0200 LT in Alaska.

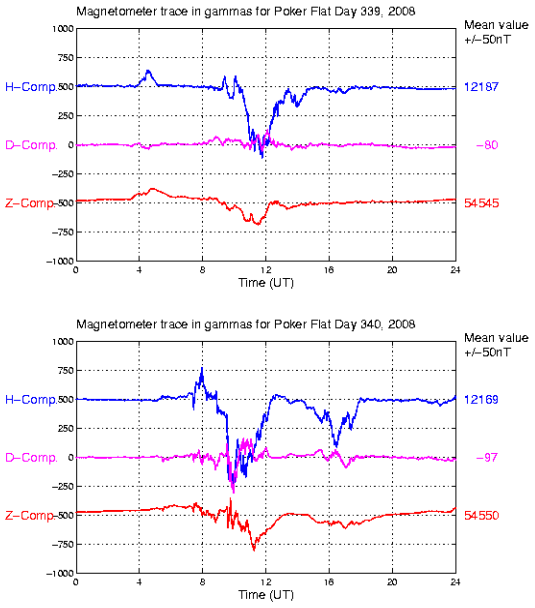

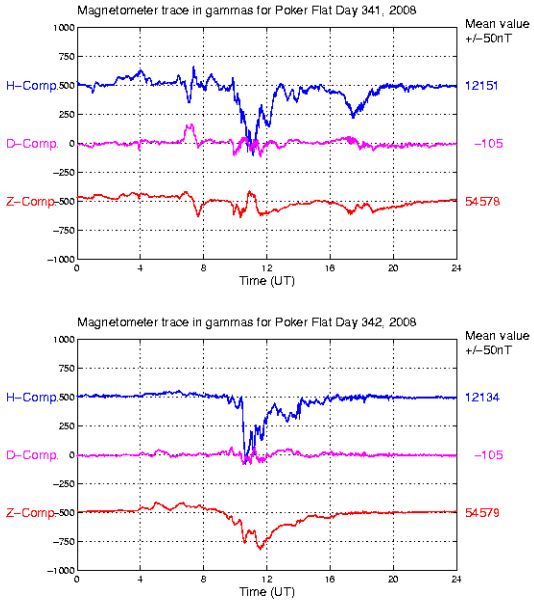

Figure 13 Geomagnetic field measured at Poker Flat from 4 December (Day 339) to 7 December (Day 342) 2008 [GIMA, 2009]

Disturbed ionosphere periods are also selected using other high latitude magnetometer stations. Based on magnetometer observations of the entire Canadian region, corresponding COSMIC RO measurements are selected during the period 4-7 December 2008. Spatial distribution and periods of disturbances are identified using GIMA, CARISMA and GSC data. Figure 14 is derived from the selected electron density observations at altitudes 100-120 km for night time sectors of the four days. Four days of observations are included because there are not enough COSMIC RO measurements for a single day to create a full electron density map. A plot is compiled from all electron density measurements during disturbed periods for the given interval of local time. COSMIC electron density observations within the same geomagnetic latitude and local time sector bins are averaged to derive the grid of values in Figure 14.

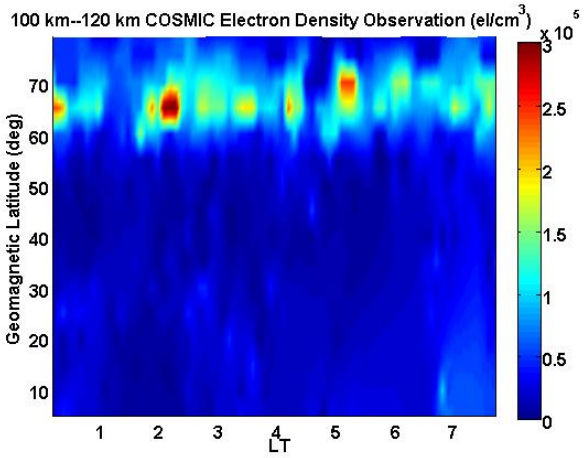

Figure 14 COSMIC electron density observations for altitude range 100-120 km generated from COSMIC

measurements 0100-0700 LT for four days (4-7 December 2008)

Electron density observations are selected for altitudes 100-120 km (corresponding to the altitude of AEI). In Figure 14 all density enhancements generally occur above geomagnetic latitude 60 deg N; this is near the equatorward boundary of the auroral oval. Localized electron density enhancements are from 2-3 $\times 10^5$ el/cm^3.

The correlation between magnetometer observations and spatial distribution of electron density enhancement is consistent with the expected occurrence of AEI during geomagnetic disturbances and associated auroral substorms. RO events from COSMIC are able to capture the AEI feature from vertical electron density profiles directly.

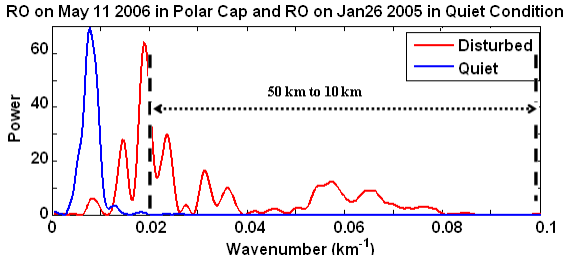

Figure 15 Power spectral density for COSMIC electron density profile

To better establish the occurrence and distribution of AEI at high latitudes, maps of intensity from power spectral analysis are shown for densities at smaller wavelengths. Figure 15 shows PSD comparisons for a “quiet” RO electron density profile and a “disturbed” electron density profile. One region is selected for analysis: wavelengths of 10-50 km; this reflects medium scale size structures. This range includes wavelengths dominant in previous analysis of AEI profiles (e.g. Figure 12); the goal of this analysis is to capture the distribution of such smaller electron density structures. The average spectral density value is computed and normalized to determine geographic distribution using the COSMIC electron density observations from ionospheric disturbed periods.

Power spectral densities for electron density values in Figure 14 for the limited wavelength range 10-50 km are shown in Figure 16. Larger values in Figure 16 demonstrate good correlation with the larger electron density enhancements at altitudes 100-120 km in Figure 14.

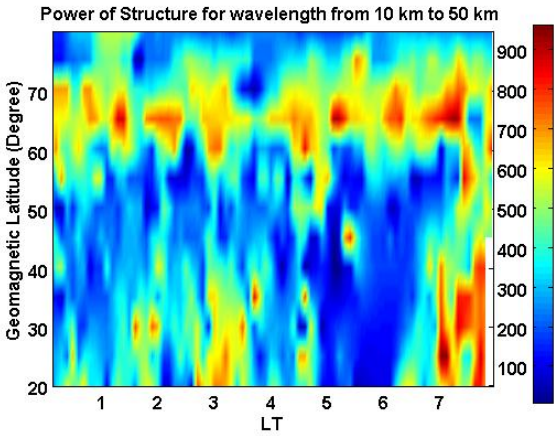

Figure 16 Power spectral density values for electron density structures with scale sizes in the range 10-50 km as derived from COSMIC measurements (4-7 December)

Prominent structures with scale size 10-50 km are observed within the auroral boundaries defined in Figure 14. This implies that the occurrence of medium-scale structures corresponds with presence of nightside AEI. It is noted that there are also regions of high spectral density at latitudes below the auroral oval boundary. However the dominant distribution of medium-scale structures at auroral latitudes (and corresponding to AEI) is evident.

CONCLUSIONS

In this work typical auroral substorm events are selected to determine if AEI can be identified from RO observations. Electron density maps are estimated from COSMIC observations to capture the extension of auroral boundaries during ionospherically disturbed periods.

GPS radio occultation measurements onboard LEO satellites demonstrate potential as a powerful tool for studying 3D electron density in the high latitude ionosphere. A drawback is that there are insufficient COSMIC RO events available per day to achieve continuous global coverage. However, improved coverage can be expected for COSMIC2 with 12 LEO satellites. Better spatial coverage can be maintained for ionospheric tomography.

A significance of the work is identifying E-region electron density enhancements during auroral scintillation periods. From COSMIC observations the presence of precipitating energetic electrons during auroral substorms is identified; scintillations develop in the region of AEI processes. For high latitude scintillation simulations for GPS applications a simple phase screen model assuming concentration of electrons in F region is not realistic. A more complex physics-based model is more realistic for high latitude scintillation modeling.

References

Anthes. R. A, P. A. Bernhardt, Y. Chen, L. Cucurull, K. F. Dymond, D. Ector, S. B. Healy, S.P. Ho, D. C. Hunt, Y.H. Kuo, H. Liu, K. Manning, C. McCormick, T. K. Meehan, W. J. Randel, C. Rocken, W. S. Schreiner, S. V.

Sokolovskiy, S. Syndergaard, D. C. Thompson, K. E. Trenberth, T.K. Wee, N. L. Yen, and Z. Zeng (2008), The COSMIC/FORMOSAT-3 mission: Early results, Bulletin of the American Meteorological Society, Vol.89(3), pp.313-333

Baron, M.J. (1974), Electron density within aurora and other aurora E-region characteristics, Radio Science, Vol.9, No.2, pp.341

Basu, S., K. M. Groves, S. Basu, and P. J. Sultan (2002), Specification and forecasting of scintillations in communication/navigation links: current status and future plans, Journal of Atmospheric and Solar-Terrestrial Physics, Vol. 64, pp.1745.

Bates, H.F., A. E. Belon and R.D. Hunsucker (1973), Aurora and poleward edge of the main trough, Journal of Geophysical Research, Vol. 78, no. 4684

CARISMA (2009), http://bluebird.phys.ualberta.ca/carisma/, accessed at 17:05 Aug 24, 2009

Coker, C., R. Hunsucker and G. Lott(1995), Detection of auroral activity using GPS satellites, Geophys. Res. Lett., Vol 22, pp.3259–3262.

COSMIC (2009) http://cosmic-io.cosmic.ucar.edu/ accessed on Jun 30, 2009

GIMA (2009), http://magnet.gi.alaska.edu/, accessed on Aug. 20, 2009

GSC (2009), http://geomag.nrcan.gc.ca/, accessed on Aug, 18, 2009

Feldstein, Y.I. (1967), Dynamics of auroral belt and polar geomagnetic disturbances, Plant Space sci., Vol.15, pp. 209-229

Hunsucker, R.D and J.K. Hargreaves (2003), The high-latitude ionosphere and its effects on radio propagation, *Cambridge University Press*

Hunsucker, R. D., C. Coker, J.A. Cook, and G.Lott (1995), An Investigation of the feasibility of utilizing GPS/TEC signatures for near-real time forecasting of auroral-E propagation at high-HF and low-VHF frequencies, IEEE Trans. on Ant. and Prop., Vol.43, pp.1313-1318

Hunsucker, R.D. (1992), Mini-review: auroral and polar-cap ionospheric effects on radio propagation, IEEE Transactions on antennas and propagation, Vol. 40, NO.7, pp.818

Ledvina, B. M., P. M. Kintner, and J. J. Makela (2004), Temporal properties of intense GPS L1 amplitude scintillations at midlatitudes, Radio Science, Vol. 39, RS1S18, doi:10.1029/2002RS002832.

Lomb, N.R. (1976), Least-squares frequency analysis of unequally spaced data, Astrophysics and Space Science, Vol.39, pp. 447-462

Mitchell, C. N, L. Alfonsi, G. De Franceschi, M. Lester, V. Romano and A. W. Wernik (2005), GPS TEC and scintillation measurements from polar ionosphere during the October 2003 storm, Geophys. Res. Lett., Vol.32, L12S03, doi:10.1029/2004GL021644

NOAA (2009), http://www.swpc.noaa.gov/, accessed on Dec 18, 2009

Rodger, A. S. and A. C. Graham (1996), Diurnal and seasonal occurrence of polar patches, Annales Geophysica, Vol.14, pp.533-537

Schreiner, S.W., C. Rocken, S. Sokolovskiy, S. Syndergaard and D. Hunt (2007), Estimates of the precision of GPS radio occultations from the COSMIC/ FORMOSAT-3 mission, Geophys Res Lett, Vol.34, L04808, doi:10.1029/2006GL027557

Schreiner, S.W., S. Sokolovskiy and C. Rocken (1999), Analysis and validation of GPS/MET radio occultation data in the ionosphere, Radio Science, Vol.34, No.4, pp.946-966

Skone, S., M. Feng and R. Tiwari, A Coster (2009), Characterizing ionospheric irregularities for auroral scintillations, Proceedings of the 22nd International Technical Meeting of the Satellite Division of the Institute of Navigation (ION GNSS 2009 Savannah, GA), September 2009, pp. 2551-2558

Skone, S., M. Feng, F. Ghafoori and R. Tiwari (2008), Investigation of scintillation characteristics for high latitude phenomena, Proceedings of the 21st International Technical Meeting of the Satellite Division of the Institute of Navigation (ION GNSS 2008 Savannah, GA), September 2008, pp. 2425-2433

Skone, S. (1998)., Wide area ionospheric grid modeling in the auroal region, UCGE Report Number 20123, Ph.D thesis, University of Calgary, Calgary, Alberta, Canada

Tsybulya, K. and N. Jakowski (2005), Medium- and small-scale ionospheric irregularities detected by GPS radio occultation method, Geophys Res Lett, Vol.32, doi:10.1029 /2005GL022420

Wu, D. L (2006), Small-scale fluctuations and scintillations in high-resolution GPS/CHAMP SNR and phase data, Journal of Atmospheric and Solar-Terrestrial Physics, Vol.68, pp.999-1017

Yu, W. (2007) Selected GPS Receiver Enhancements for Weak Signal Acquisition on Tracking. Msc Thesis, published as Report No. 20249, Department of Geomatics Engineering, The University of Calgary